Available online at www.sciencedirect.com

ScienceDirect

Journal of the European Ceramic Society 30 (2010) 689–697

www.elsevier.com/locate/jeurceramsoc

Mechanical properties of PECVD thin ceramic films

Ghatu Subhash [a,*], Philip Hittepole [b], Spandan Maiti [b]

[a] Mechanical and Aerospace Engineering, University of Florida, Gainesville, FL 32611, USA

[b] Department of Mechanical Engineering-Engineering Mechanics, Michigan Technological University, Houghton, MI 49931, USA

Received 9 July 2009; received in revised form 8 September 2009; accepted 17 September 2009
Available online 12 October 2009

Abstract

Silicon dioxide (thickness 350 nm and 969 nm) and silicon nitride (thickness 218 nm) films deposited on silicon substrate using plasma enhanced chemical vapor deposition process were investigated using a Berkovich nanoindenter. The load-depth measurements revealed that the oxide films have lower modulus and hardness compared to the silicon substrate, where as the nitride film has a higher hardness and slightly lower modulus than the substrate. To delineate the substrate effect, a phenomenological model, that captures most of the 'continuous stiffness measurement' data, was proposed and then extended on both sides to determine the film and substrate properties. The modulus and hardness of the oxide film were around 53 GPa and 4–8 GPa where as those of the nitride film were around 150 GPa and 19 GPa, respectively. These values compare well with the measurements reported elsewhere in the literature.
© 2009 Elsevier Ltd. All rights reserved.

Keywords: Ceramic films; PECVD; Nanoindentation; CSM; Modulus and hardness

1. Introduction

Ceramic oxide and nitride films are used extensively as structural members such as flexible membranes, tunable inductors, tunable optical filters, etc., in MEMS devices.[1,2] Nitride and oxide stacked layers are also used as gate dielectrics in microelectronics, in thin film transistors and in metal–oxide semiconductor integrated circuits.[3,4] In semiconductor industry, silicon dioxide (SiO_2) and silicon nitride (Si_3N_4) films are used as masking materials to isolate active circuits from each other and to provide mechanical and chemical protection during fabrication of devices using chemical vapor deposition (CVD) techniques. Further applications of nanofilm materials are envisioned in ultra small and lightweight bio- and chemo-sensors. Rare-earth oxide doped thin film coatings are also used for field emission display devices in electronic industries.[5] Coatings that alter tribological properties and extend lifetime of biological implants and computer hard disks, and patterned dichoric coatings for optical filters are some of the prime examples[6] of this emerging concept. Many of these applications require nano-thickness materials with highest quality, reproducible characteristics and reliability.

Although the principal function of thin film components are often non-structural,[7] these membranes frequently carry mirrors and operate under electrostatic forces to deflect them in response to applied bias voltage.[1] Thus, the mechanical characterization of thin films is essential for determination of structural integrity and performance. Nonetheless, the processing method associated with the manufacture of these materials often introduces residual stresses sufficient to induce mechanical deformations that can lead to performance degradation and/or malfunction in electrical, magnetic and optical properties of this class of materials.[8] Thus, characterization of mechanical deformation and understanding of failure behavior of nanofilm materials is an important first step to insure mechanical integrity, reliability under operating and adverse conditions, and proper performance of various micro- and nano-devices.

Unfortunately, the determination of mechanical properties of thin films is non-trivial because of their small dimension along the thickness direction. For many applications, the film thickness is of the order of a few tens or few hundred nanometers while the lateral dimensions can be several hundred times greater. Owing to this small thickness, the properties of these materials are significantly different than their bulk counterparts, and standard methods of testing bulk materials cannot be employed successfully at this length scale. Moreover, thin film property determination using indentation techniques uti-

* Corresponding author. Tel.: +1 352 392 7005.
E-mail address: subhash@ufl.edu (G. Subhash).

0955-2219/$ – see front matter © 2009 Elsevier Ltd. All rights reserved.
doi:10.1016/j.jeurceramsoc.2009.09.020

lizes very small sample volume which is also prone to influences from the substrate properties even at depths smaller than one-tenth of film thickness.[9] Also, it is now well recognized that the properties of these thin films vary with processing scheme. For example, Young's modulus of silicon nitride (Si_3N_4) thin films varies between 97 GPa and 210 GPa depending on the processing scheme.[1,4] Therefore, determination of film properties is essential whenever a new process is adopted to produce thin films. At small thicknesses, the influence of surface roughness, substrate behavior and mismatch between the film and substrate properties further complicate the mechanical characterization processes. As a result, the experimentally obtained material properties exhibit considerable scatter depending on the techniques used,[7] thus rendering the usefulness of measured parameters somewhat limited.

Numerous mechanical testing techniques, such as micro-tension tests[10,11] and micro-cantilever bend tests[12] have been used to determine the mechanical properties of such thin films. The advantage of these tests is their similarity to conventional macro-scale tests and ease of property determination. The disadvantage is the high level of cost in developing such micro-test devices and the design of test specimens. However, in recent years, instrumented nanoindentation technique has emerged as a powerful experimental alternative to the above techniques due to its simplicity and its requirement of small material volume during the test.[13–17] This technique allows precise control of either load or displacement during the test and allows for experimental measurements on small samples by subjecting them to loads as low as a few micro-Newtons and at depths in the nanometer range. Mechanical properties such as elastic modulus (E) and hardness (H) of the film can be extracted from a record of load–displacement (p–h) curves.[18–20] Characterization of a single layer deposited on a substrate has been the focus of numerous investigation.[7,15,21–28] However, the methods adopted are still under scrutiny and are not universally applicable. Most of the above investigations are also focused on metallic films and similar results on a range of ceramic films are not widely available yet. Ceramic thin films, being brittle in nature, behave in a considerably different manner than their metallic counterpart. In this article, we explore the nanoindentation technique to determine properties of thin ceramic films of various thicknesses. We also suggest a new empirical relationship relating materials properties and indentation depth that allows us to evaluate stiffness and hardness of ceramic thin films. Effect of substrate properties can be clearly delineated from that of the film using this relationship. By choosing suitable thicknesses of films and conducting systematic nanoindentation experiments at various depths, we have been able embark on a procedure to isolate the influence of the substrate and effectively determine the properties of thin films.

2. Materials

Two silicon dioxide (SiO_2) films of thickness 348 nm and 969 nm, and one silicon nitride (Si_3N_4) film of thickness 218 nm, all deposited separately on single crystal silicon (Si) wafers were obtained from Army Research Laboratories, Adelphi, MD. Each of these dielectric films was deposited using plasma enhanced chemical vapor deposition (PECVD) process in a Plasma-Therma 790 deposition chamber operating at a pressure of 900 mT and a temperature of 250 °C using appropriate precursor gases. The precursor gases for the Si_3N_4 film were silane (SiH_4), nitrogen (N_2), and ammonia (NH_3) with helium (He) as a carrier gas, and for the SiO_2 film the precursor gasses were SiH_4 and nitrous oxide (N_2O) with He as the carrier gas. Following the deposition process, the substrates were annealed at 700 °C for 60 s in flowing N_2 so as to remove trapped hydrogen from the films and to stabilize the residual stress state within the films. The film thickness was measured at 33 locations across the wafer using a multi-angle multi-wavelength ellipsometer. The wafers were then diced into quarters with one quarter diced into 4 mm × 4 mm samples and another quarter diced into 6 mm × 6 mm samples following application of an AZ5200 series photoresist.

3. Experimental approach

Nanoindentation experiments were conducted using an MTS Nanoindenter® RXP equipped with a Berkovich diamond indenter (tip radius of 100 nm). The indenter was calibrated using fused silica as the standard. On average, ten indentations were performed at each depth for six depths ranging from 20 nm to approximately twice the film thickness. The continuous stiffness measurement (CSM) option was used at each depth. This option superposes an oscillation on the load signal to continuously monitor the surface stiffness and provides data on film stiffness (E) and hardness (H) values as a function of depth (h) of indentation. The CSM signal was set to an amplitude of 2 nm at a frequency of 45 Hz. The indenter tip was set to approach the film surface at a velocity of 5 nm/s from a distance of approximately 1000 nm. Surface contact was determined by a measured increase in contact stiffness by 40–50% of the presumed surface stiffness of 80 N/m. The indenter was allowed to continue penetration on the surface at a target strain rate of 0.050/s. Once the indenter reached the prescribed indentation depth, it was held at that load for 10 s. The indenter was then withdrawn at the maximum loading rate until the load on the sample was 10% of the maximum load achieved. Around 10 indentations were performed at each depth for each film thickness. Some additional indentations were also performed at selected depths on Si substrate for comparison to the film properties. All the indentations were later interrogated using both a field emission scanning electron microscope (FE-SEM) and an atomic force microscope (AFM). The FE-SEM was used primarily for characterization of the indentations, including crack pattern determination. The AFM was used for profiling the indentations for determining the residual depths, and whether pile-up occurred around the indents.

3.1. Experimental results

3.1.1. p–h curves

Load–displacement (p–h) curves at various depths on Si_3N_4 and SiO_2 films along with those on Si substrate are shown in Fig. 1(a) and (b), respectively. For clarity, only one curve at

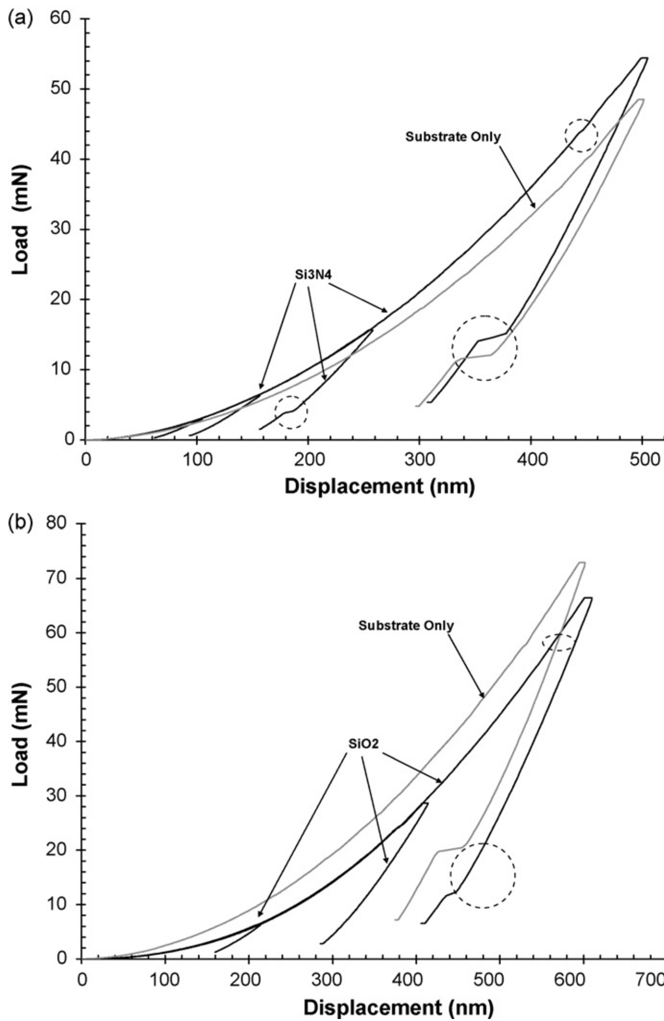

Fig. 1. Load–displacement (*p*–*h*) curves for different depths on (a) Si_3N_4 (218 nm) and (b) SiO_2 (348 nm) films indicating pop-ins during loading and unloading.

selected depths for each film, and for comparison purposes, one curve on Si substrate at the maximum depth are shown in each figure. Clearly, the load required on Si_3N_4 film at any penetration depth is greater (Fig. 1(a)) and that required on SiO_2 film is lower (Fig. 1(b)) than that on Si substrate. This result was consistently observed at all the depths chosen for the study. As will be seen later in discussions on hardness measurements that, this result will lead us to confirm that the nitride film is harder than the Si substrate and the oxide film is softer than the substrate. One distinct feature in all the *p*–*h* curves is the sudden displacement jumps (called 'pop-in') during the loading as well as the unloading phases of indentation, as indicated by circles. These features are attributed to cracking in the film as will be discussed in the following section. In general, these displacement jumps were more frequent, were of larger amplitude, and occurred even in lower depth *p*–*h* curves in nitride film than in oxide films. This observation leads us to believe that the Si_3N_4 film was more brittle than the SiO_2 film.

The SiO_2 film of higher thickness (969 nm) was also subjected to indentations at multiple depths, with the deepest indentations at nearly twice the film thickness. *p*–*h* curves at the selected three different depths of indentation are shown in Fig. 2. The loading paths of different *p*–*h* curves coincide well up to a depth of approximately 1200 nm, after which they begin to diverge. There is a displacement jump (pop-in) at around 1000 nm, followed by a number of additional small pop-ins in both loading and unloading phases. The pop-in at 1000 nm could be an effect of film cracking or delamination after which the two curves start to diverge all the way to a maximum depth of 1800 nm. The evolved cracking patterns in these ceramic films are discussed in the following.

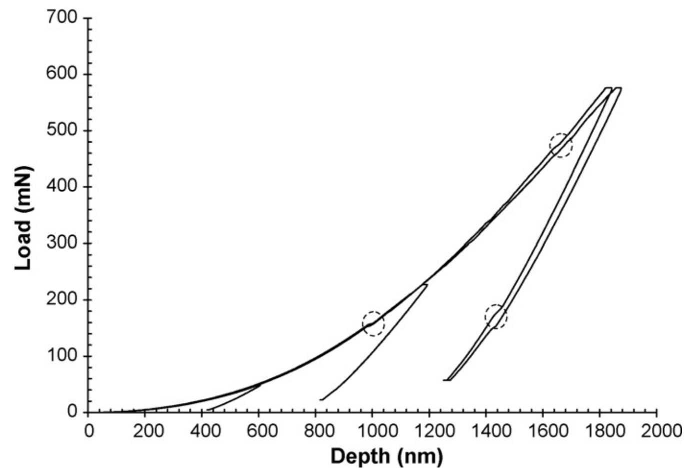

Fig. 2. Load–displacement (*p*–*h*) curves for different depths on thick (969 nm) SiO_2 films indicating pop-ins during loading and unloading.

3.1.2. Cracking in thin films

Microscopic observation of nitride films subjected to various depths of indentations revealed radial cracking at lower loads followed by edge cracking and large lateral cracking at higher indentation loads. The radial cracks, seen in Fig. 3(a), occur due to the stress concentration induced by the sharp pyramidal edges of the Berkovich indenter. These cracks can extend beyond the contact region. As the load is increased, edge cracks start to form along the base of the indent connecting two radial cracks, see Fig. 3(b). Thus the film starts to break into triangular strips. With increase in load, additional edge cracks emerge parallel to the first set of edge cracks as seen in this micrograph. Emergence of such cracks can lead to sudden displacement jumps in the *p*–*h* curves during the loading phase. Upon unloading the stress starts to decrease but the inelastic deformation induces residual tensile stress.[29,30] This was also confirmed by finite element simulations of the indentation process.[31] This tensile stress causes lateral cracks to develop as seen in the Fig. 3(c) and contributes to displacement jumps during unloading phase of indentation. The evolution sequence of these radial and lateral crack systems have been extensively studied in the indentation literature on brittle materials.[29,30,32] More recently, Musil and Jirout[33] have investigated the relationship between cracking of films in relation to mechanical properties, the structure of film and the substrate. They found that resistance to cracking increases with increasing ratio H^3/E^{*2} of film where E^* is the effective modulus given by $E(1-v^2)$ and v is the Poisson's ratio of film. Interestingly they

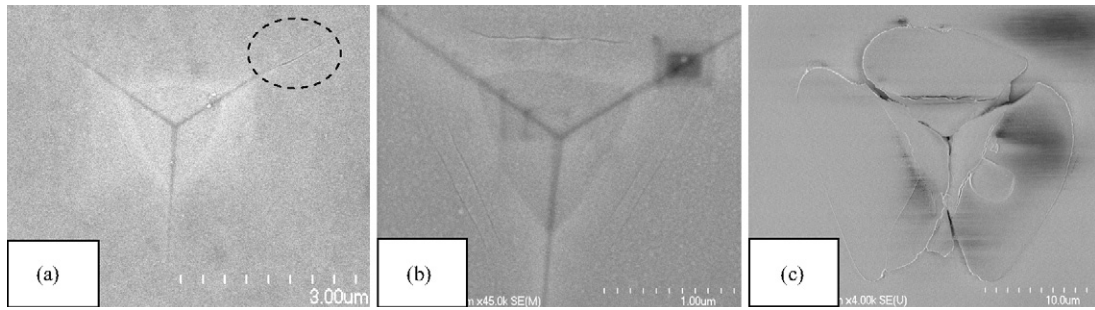

Fig. 3. Cracking patterns in Si_3N_4 film revealing (a) radial cracking, (b) edge cracking and (c) lateral cracking in SiO_2 film.

found that cracking of film does not occur until a critical depth is achieved. The propensity for cracking is also influenced by the substrate properties.

3.1.3. Hardness and modulus measurements

The continuous stiffness measurement (CSM) technique employed in the current investigation in the Nanoindenter® allows for measurement of modulus and hardness at various depths of indentation. Fig. 4 shows the data for all three materials on instantaneous modulus (the continuous curve) averaged from ten CSM measurements until the maximum depth of indentation is reached. Also shown is the modulus data at each depth from unloading curves averaged over 10 such indents. Notice that the discrete data at lower maximum depths matches well with the CSM curve all the way to the final maximum depth of nearly twice the film thickness. The modulus of Si substrate and that of Si_3N_4 film appear to be almost the same, but both these measurements are significantly greater than the measured values on oxide film. However, beyond certain depth the modulus measured from the two SiO_2 films continues to diverge with depth of indentation. The stiffness of the thin SiO_2 film ($t = 350$ nm) increases at a faster rate with depth than that of the thicker SiO_2 film ($t = 969$ nm). This result clearly indicates that the influence of substrate is felt very early in a thinner film during the indentation process and hence the stiffness rapidly tends towards the substrate value with increasing depth of indentation. Interestingly, even at a depth close to twice the film thickness, the modulus measured on the thick ceramic film does not reach that of the substrate. This behavior may be due to the larger volume of the film in contact with the indenter and still resisting the indentation load at these depths compared to the small volume of the substrate materials resisting the indentation closer to the indenter tip. At these depths the influence of substrate is higher on thin films than on a thicker film. These issues will be discussed in more detail in Section 3.

Similar to the data on modulus in Fig. 4, the hardness measurements for the three films and the substrate are shown in Fig. 5. As noted earlier in *p–h* curves (Fig. 1), the hardness of Si_3N_4 film is significantly greater and that of SiO_2 films is significantly lower than that of the Si substrate whose hardness stabilizes at around 13.2 GPa for depths greater than 300 nm. At lower depths, the nitride film shows a high hardness reaching up to 18 GPa and as the depth of indentation increases the hardness tends towards the substrate value. On the other hand, the hardness of the oxide films is lower than that of the substrate. With increasing depth of indentation, the hardness of the thinner film ($t = 348$ nm) tends faster towards that of the Si substrate than the thicker ($t = 969$ nm) SiO_2 film, similar to the trends observed in Fig. 4 for modulus measurements.

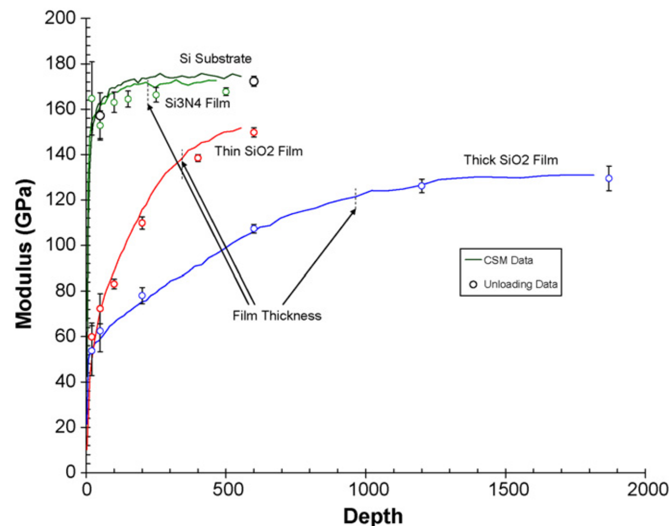

Fig. 4. Instantaneous modulus measurements from CSM and unloading data at fixed depths for the ceramic films.

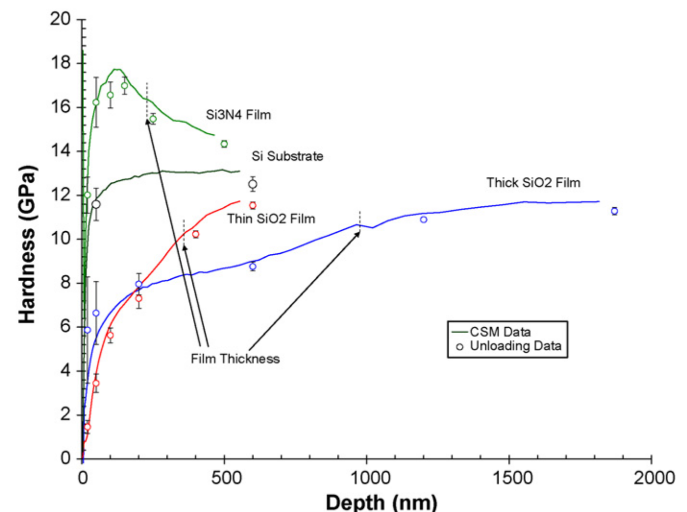

Fig. 5. Instantaneous hardness measurements from CSM and unloading data at fixed depths for the ceramic films.

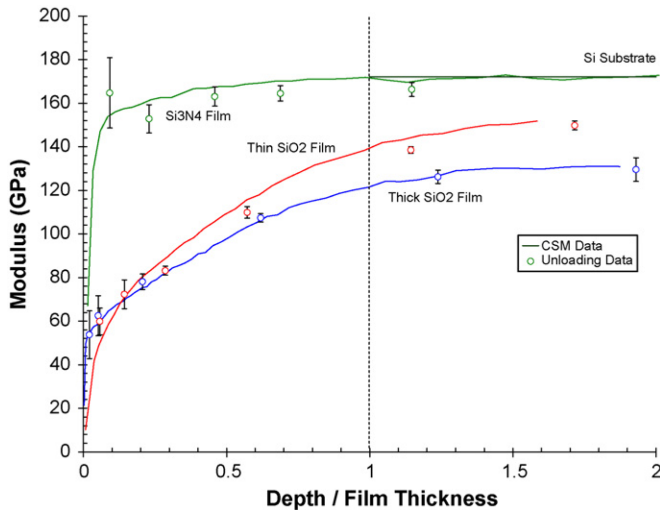

Fig. 6. Modulus measurement as a function of normalized indentation depth.

To better rationalize these results, the above modulus and hardness measurements are plotted as a function of normalized thickness in Figs. 6 and 7, respectively, where the depth of indentation is normalized with the thickness of the corresponding ceramic film. Clearly, at large depths the properties for all the films appear to tend towards the substrate properties. In the case of SiO_2 films, the modulus values do not reach that of the substrate even at a depth twice that of the total SiO_2 film thickness (see Fig. 6), where as the modulus of the nitride film reaches the substrate value fairly quickly and remains at that value for greater depths. Similarly, the hardness values are plotted in Fig. 7 as a function of normalized depth. Despite different thicknesses, both the SiO_2 films seem to monotonically tend towards the substrate value. Obviously, the measured values on the thinner film tends towards the substrate value faster than the values measured on the thicker film. On the other hand, the nitride film reaches a peak and then gradually tends towards the substrate. In all these cases, it is difficult to approximate the depth at which the substrate properties start to influence the measured film properties.

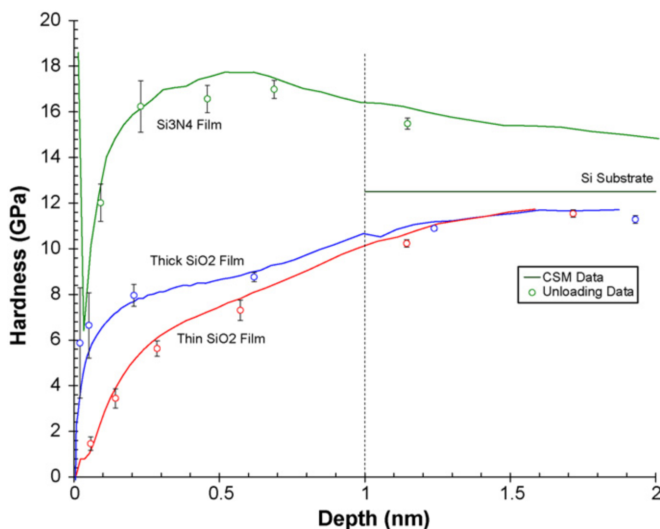

Fig. 7. Hardness measurements as a function of normalized indentation depth.

More in-depth analysis will be attempted using modeling studies described in Section 3.

One of the major limitations in using nanoindentation technique for thin film property determination is that film properties cannot be directly determined from this test method because the data obtained from such tests is strongly influenced by the substrate properties. Separation of film properties from this data is not straightforward. Martinez et al.[14] advocated development of nanoindentation stress–strain curves using four indenter geometries for complete mechanical characterization. This method is rather complex and time consuming. Chen et al.[15] asserted that the non-linearities in a plot of unloading slope versus normalized depth (h/t) reveal a transition from film-dominated to substrate-dominated behavior and these non-linearities can be used to extract the film properties. This method works only when film and substrate stiffnesses are comparable and the film is thick enough to show film-dominated behavior during early phase of indentation. However, thin films behave differently than their bulk counterparts in many regards. Because they are thin and are bonded to a substrate, material parameters such as interfacial cohesive strength and interfacial fracture toughness may also influence the measured properties. There is also, presumably, a size effect due to film thickness. Dislocations are bounded not only by the free surface, but also by the interface. As the film thickness decreases in crystallographic films, dislocations become more tightly constrained. This can lead to increased hardness and increased strain hardening rates compared to thicker films and bulk materials. Most recently, Manika and Maniks[9] presented a detailed analysis of critical indentation depth criteria for film hardness determination by varying the coating/substrate hardness ratio from 0.01 to 20 and concluded that the critical indentation depth depends not only on film–substrate properties but also on film substructure.

The discussion above pertains to the indentation response of metallic films. Ceramic thin films exhibit different deformation behavior owing to their brittleness. However, compared to metallic thin films, relatively little work has been conducted on nanoindentation response of ceramic thin films, although significant progress has been accomplished in recent years. Huang et al.[1] found a simplified method of empirically separating the film and substrate modulus using a power-law curve fit on SiN_x films. Vila et al.[4] experimentally determined property variations in Si_3N_4 films due to processing methods and found that E and H can vary by a factor of about 2. Soh et al.[28] performed very shallow ($h/t \approx 10\%$) nanoindentations on a-SiN_xH_y films and showed that substrate influence was significant from the very beginning and this can be seen as a substantial variation in the load–deflection curves, which is often attributed to factors such as surface roughness. Due to the above difficulties and limitations, in the following, we will resort to empirical modeling efforts to identify the film properties and make comparisons to the published values available elsewhere in the literature.

4. Phenomenological modeling

There have been numerous efforts in the literature to extract properties of thin films from the limited experimental load–depth

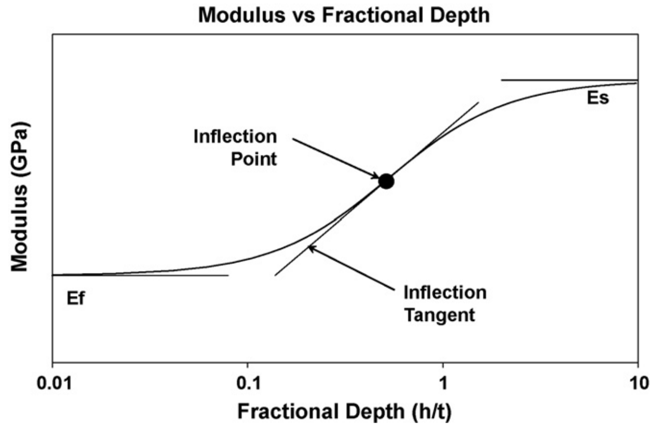

Fig. 8. Schematic plot revealing the behavior of film–substrate system with indentation depth.

data during indentations. The biggest challenge seems to be the identification of depth at which the substrate properties become dominant. The typical approach is to propose an equation to fit the experimental data and extrapolate the film and substrate properties from the model. For spherical indenters a phenomenological model was developed by Hu and Lawn[34] to describe the transition of mechanical properties from film dominance to substrate dominance. This model was later adapted to Berkovich indenters by Jung et al.[35] They introduced the following equation for Young's modulus as a function of normalized indentation depth, $E(h/t)$, with boundary condition $E(0) = E_f$:

$$E = E_s \left(\frac{E_f}{E_s} \right)^{(1+A(h/t)^B)^{-1}} \tag{1}$$

where A and B are fitting parameters, t is film thickness and h is indentation depth. E_f and E_s are Young's moduli of film and substrate materials, respectively. Huang et al.[1] introduced a similar but slightly simplified equation as

$$E = E_s \left(\frac{E_f}{E_s} \right)^{1-e^{-A(h/t)}} \tag{2}$$

Clearly, both equations provide slightly different control over the ability of the equation to fit the experimental data. The intent of both the equations is to capture the film response at low depths and that of substrate response at high depths. Thus, the measured data follows an *s*-shaped curve (on a plot of h/t versus E) which is bounded by two asymptotes that represent film and substrate properties, see Fig. 8. In Eq. (1) by Jung et al.[35] the parameter A affects the h/t value of the inflection point (or h/t-intercept of the inflection tangent), while B controls the slope of the tangent at the inflection point. It should be noted that, for a given E_s/E_f, changing A while holding B constant changes only the h/t value of the inflection point (or h/t-intercept). On the other hand, changing B while holding A constant affects both the slope and h/t-intercept. This is because B does not rotate the inflection tangent about the inflection point (or h/t-intercept) where as, in Eq. (2), A controls the h/t value of the inflection point, but there is no control over the inflection slope (the target value). Raising h/t to the B power would add control of the inflection slope to this equation. The slightly different forms of these equations obviously result in somewhat different curves and different extrapolated values of the film and substrate. The Huang et al.[1] equation results in sharper transitions between the upper and lower asymptotes and the inflection tangent compared to that of Jung et al.[35]

Here, we propose another relationship that will provide the benefits of both the above equations as

$$E = E_f + (E_s - E_f) \left(\frac{e^{A(h/t)} - 1}{e^{A(h/t)} + B} \right) \tag{3}$$

The parameters A and B have the same role as in Eq. (1), but with a response more similar to Eq. (2). We will now utilize the large set of data from CSM (Figs. 4 and 5) and the unloading slopes at fixed depth indentations (Figs. 1 and 2) along with the above model results to extract the film and substrate properties. Note that we already have the substrate (Si) properties determined from separate nanoindentation tests (Figs. 1–7). These values provide one asymptote for the model, i.e., substrate properties at large indentation depths ($h/t \gg 1$). The film property, yet to be determined, marks the second asymptote value at low depths. The measured data from the nanoindentation tests falls in between these two values in a narrow range due to the assumed substrate influence at various depths. By anchoring the curve at the first asymptote (i.e., substrate value) and adjusting the parameters in the model such that the curve captures most of the experimental data, the film properties are extrapolated at zero depth.

The raw data in terms of CSM values, measurements from unloading curves at prescribed depth, and a power-law curve fit for CSM data are all shown in Fig. 9(a). First, we will illustrate the model results for the thick ($t = 969$ nm) SiO_2 film. In Fig. 9(b) it is seen that all the models (Eqs. (1)–(3)) capture most of the experimental data reasonably well. Both Huang et al.[1] and the current model (referred to as Subhash et al.) extrapolate the curve to a film modulus of (E_f) of 53 GPa where as Jung et al., model gives slightly higher value of 56 GPa. The latter model fails to reach the substrate value at the other end even at a depth ten times the film thickness. The model results for the remaining two films are shown in Fig. 9(c) and (d). Unlike the results on thick SiO_2 film, the models do not fully capture the experimental data on thinner films, especially at depths below one-tenth of the film thickness. At such low depths (or low loads) recent analysis by Pharr et al.[20] revealed that the indenter is not always in contact with the specimen during CSM mode. Recall that in the CSM mode the indenter is unloaded periodically to gather the instantaneous unloading slope. This unloading phase is of the order of few nanometers. At extremely small indentation depth, the unloading depth is comparable to (and some times exceeds) the indentation depth and hence the indenter looses contact with the specimen. When the CSM mode is turned off (i.e., operated in continuously increasing depth mode), the indenter is always in contact with the specimen during the loading phase of indentation. Thus, both the load and the depth measurements at low depths are not the same with and without the CSM option. Correction factors are being developed for measurements at such

Fig. 9. Comparison of results for modulus of film and substrate: (a) power-law model fit for the modulus data, (b) SiO_2 film (t = 969 nm), (c) SiO_2 film (t = 348 nm) and (d) Si_3N_4 film.

extremely low depths during the CSM mode.[20] Even these correction factors have limitations and cannot be applied below a suggested critical value. Such procedures are not fully available and hence the correction factors could not be applied for the current data. In addition, there are other reasons for not utilizing the low-depth data. At extremely small indentation depths, surface features such as asperity height on the films and the resulting surface roughness influence the indentation behavior due to their comparable length scale to the depth of indentation and indenter curvature. Chen et al.[26] attributed the initial increase in hardness for metallic thin films at extremely low depths to strain gradients effects. Recent investigations by Manika and Maniks[9] found that even film substructure such as grain boundaries and interfacial strength also strongly influence the measured values. Therefore, the experimentally derived hardness or modulus values at extremely small loads (and depths) may not be reliable.

Similar to the thick SiO_2 film results presented in Fig. 9(b), the models on thin SiO_2 film, shown in Fig. 9(c), also result in film modulus of 53 GPa. However, different values of A and B are required to describe the two responses. This result may imply that the influence of substrate occurs in the measurements to a varying degree at the same normalized depths on two films of same material but of different thickness. This behavior is expected because for a thinner film (t = 348 nm) the influence of substrate initiates early and for thicker film (t = 969 nm) the influence initiates at a much later depth. The data presented here clearly reflects this trend and is captured by the models effectively, i.e., all the models fit the experimental data on the thinner film at higher depths where substrate properties dominate and on thicker film at lower depth where the film properties dominate. For Si_3N_4 film, shown in Fig. 9(d), the modulus is determined to be around 150 GPa. A similar analysis was also performed on hardness data as shown in Fig. 10. Once again the

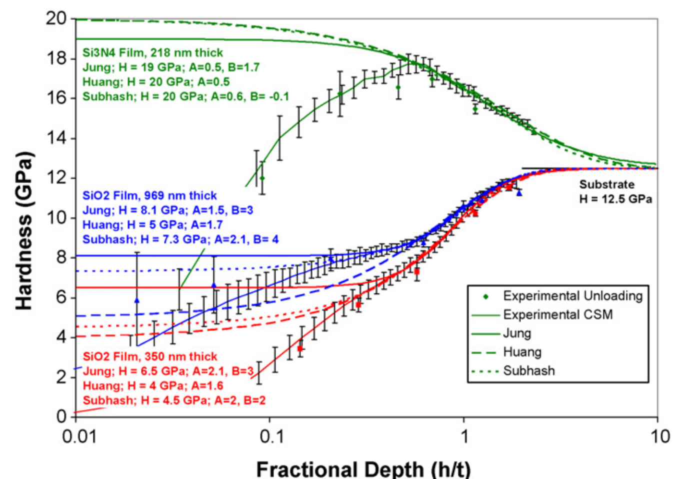

Fig. 10. Comparison of results for hardness of film and substrate from various models.

Table 1
Hardness and modulus values for ceramic films.

Property	Material	Current study (GPa)	Other studies (GPa)	Material	Reference
Young's modulus (GPa)	Si	172 (d > 100 nm)	168	Si; d > 40 nm	1
			177	Si⟨1 0 0⟩	38
			179	Si⟨1 0 0⟩; d = 24 nm	6
			202	Si⟨1 0 0⟩; d = 267 nm	6
	SiO_2	53	46–68	Thermal-wet grown SiO_2 (425 nm)	39
				Thermal-dry grown SiO_2 (325 nm)	
			69	Sputtered SiO_2 (400 nm)	
	Si_3N_4	150–155	97	PECVD SiN_x	1
			197	PECVD $SiN_{1.33}$	38
			118–200	Sputtered Si_3N_4	4
			104–156	Sputtered Si_3N_4 (200 nm)	39
			133+–19	PECVD SiN_x	3
			140+–26	PECVD SiN_x	3
			107–198	PECVD SiN_x	40
Hardness (GPa)	Si	12.5 (d > 20 nm)	11.9	Si⟨1 0 0⟩	38
			13	Si⟨1 0 0⟩; d = 24 nm	6
			11.9	Si⟨1 0 0⟩; d = 267 nm	6
	SiO_2	4–8.1			
	Si_3N_4	19	19.2	PECVD $SiN_{1.33}$	38
			9–19	Sputtered Si_3N_4	4
			11.4–22.1	PECVD SiN_x	40

data at lower depths (<20 nm) is not well captured by the models for the reasons described earlier.

Table 1 summarizes the extracted modulus and hardness values from the above model results along with available data in the literature on similar films. For completeness, data on Si substrate is also included. Clearly, the properties determined from this analysis on the Si substrate and the ceramic films compare well with those available in the literature. The modeling method proposed here also seems to capture the trends in the experimental data to yield appropriate values for modulus and hardness of substrate and films. It is interesting to note from Fig. 9(a)–(d) that the influence of the substrate on the derived properties is dependent on film thickness. For e.g., when film thickness is high (t = 969 nm, Fig. 9(b)) the influence of substrate is not so significant even well after a depth greater than the film thickness is reached (i.e., when $h/t > 1$). However, when film thickness is small (e.g., t = 350 nm, Fig. 9(c)), the low-depth indentations are strongly influenced by several factors such as the instrument limitations and the comparable values of surface asperities and indenter curvature with the depth of indentation. As the depth of indentation increases, the influence of these surface features is diminished but the influence of substrate starts to dominate. The transition region between these two influences is fairly narrow and lies at h/t value of around 0.1. Even in this range, the method used to determine the properties of film in relation to the substrate seems to appropriately interpret the data. For e.g., in Fig. 9(d), the data just beyond $h/t = 0.1$ is constant around 150 GPa for a small range before it starts to raise to the substrate value (E = 172 GPa) thus revealing the substrate influence on the measured data even at low depths. In literature, it has been well accepted that the substrate properties dominate when the ratio of h/t exceeds 0.1, called Buckle's one-tenth rule.[36] However, recent analysis by Manika and Maniks[9] suggests that when the film hardness is greater than the substrate hardness, more severe limits should be imposed. On the other hand, in Fig. 9(c), such a transition is masked by the continuous rise of the data where the model results coincide with the experimental data. Although similar influences can also be detected in hardness data provided in Fig. 10, the transition region seem to extend up to $h/t = 0.5$. This discrepancy is because of the way hardness and modulus are derived in the nanoindentation. While the modulus is derived from the unloading curve (which is elastic), the hardness is estimated from the depth of indentation and load, both of which are prone to error at low depth for the reasons stated earlier. Tsui and Pharr[37] have also revealed similar discrepancies in measurement of hardness and modulus by nanoindentation. They concluded that substrate also affects the unloading slope of the curve because of which both the hardness and modulus are over estimated. Nevertheless, the proposed model takes into account the majority of data in the intermediate range of h/t values to provide reasonable values for the film properties shown in Table 1. The method does not depend on the nature of materials and therefore can be applied to wide range of substrate–film combinations.

5. Conclusions

The properties of PECVD ceramic thin films deposited on silicon substrate were measured using Berkowitz nanoindenter. A phenomenological model was proposed which utilizes the experimental data and extrapolates the film properties. The analysis revealed that the modulus of SiO_2 film is around 53 GPa and that of Si_3N_4 film is between 150 GPa and 155 GPa. These moduli were lower than the substrate (Si) modulus of 172 GPa determined using the same method. The hardness measurements revealed that the hardness of SiO_2 film is between 4 GPa and 8 GPa and the hardness of Si_3N_4 film is around 19 GPa. For the Si substrate, the hardness was measured to be 12.5 GPa. These

values are in agreement with the available data in the literature. It was also found that the measured data at extremely low depths (<20 nm) and low loads cannot be used in the current method due to the uncertainties in the measurement system.

Acknowledgements

The authors are grateful to Dr. Ronald Polcawich of U.S. Army Research Laboratory, Adelphi, MD for providing the thin film samples for this research.

References

1. Huang, H., Winchester, K., Liu, Y., Hu, X., Musca, C., Dell, J. *et al.*, Determination of mechanical properties of PECVD silicon nitride thin films for tunable MEMS Fabry–Pérot optical filters. *J. Micromech. Microeng.*, 2005, **15**(3), 608–614.
2. Winchester, K. J. and Dell, J. M., Tunable Fabry–Pérot cavities fabricated from PECVD silicon nitride employing zinc sulphide as the sacrificial layer. *J. Micromech. Microeng.*, 2001, **11**, 589–594.
3. Zhou, W., Yang, J., Li, Y., Ji, A., Yang, F. and Yu, Y., Bulge testing and fracture properties of plasma-enhanced chemical vapor deposited silicon nitride thin films. *Thin Solid Films*, 2009, **517**(6), 1989–1994.
4. Vila, M., Cáceres, D. and Prieto, C., Mechanical properties of sputtered silicon nitride thin films. *J. Appl. Phys.*, 2003, **94**(12), 7868–7873.
5. Gozzi, D., Latini, A., Salviati, G. and Armani, N., Growth and characterization of red–green–blue cathodoluminescent ceramic films. *J. Appl. Phys.*, 2006, **99**(12), 123524.
6. Bhushan, B. and Li, X., Nanomechanical characterisation of solid surfaces and thin films. *Int. Mater. Rev.*, 2003, **48**, 125–164.
7. Sasaki, T., Yang, M., Fukushima, S. and Tsukano, R., Development of the CAE-assisted nano-indentation method for the evaluation of the anisotropic mechanical-properties of thin films. *J. Mater. Process. Technol.*, 2004, **151**, 263–267.
8. Freund, L. B. and Suresh, S., *Thin Film Materials, Stress, Defect Formation and Surface Evolution*. Cambridge University Press, Cambridge, UK, 2003.
9. Manika, I. and Maniks, J., Effect of substrate hardness and film structure on indentation depth criteria for film hardness testing. *J. Phys. D: Appl. Phys.*, 2008, **41**(7), 074010.
10. Huang, H. and Spaepen, F., Tensile testing of free-standing Cu, Ag and Al thin films and Ag/Cu multilayers. *Acta Mater.*, 2000, **48**(12), 3261–3269.
11. Hommel, M. and Kraft, O., Deformation behavior of thin copper films on deformable substrates. *Acta Mater.*, 2001, **49**(19), 3935–3947.
12. Weihs, T., Hong, S., Bravman, J. and Nix, W., Mechanical deflection of cantilever microbeams—a new technique for testing the mechanical properties of thin-films. *J. Mater. Res.*, 1988, **3**(5), 931–942.
13. Bull, S. J., Nanoindentation of coatings. *J. Phys. D*, 2005, **38**(24), R393–R413.
14. Martinez, E., Romero, J., Lousa, A. and Esteve, J., Nanoindentation stress–strain curves as a method for thin-film complete mechanical characterization: application to nanometric CrN/Cr multilayer coatings. *Appl. Phys. A*, 2003, **77**(3–4), 419–426.
15. Chen, S., Liu, L. and Wang, T., Investigation of the mechanical properties of thin films by nanoindentation, considering the effects of thickness and different coating–substrate combinations. *Surf. Coat. Technol.*, 2005, **191**(1), 25–32.
16. Tunvisut, K., Busso, E. P., ODowd, N. P. and Brantner, H. P., Determination of the mechanical properties of metallic thin films and substrates from indentation tests. *Philos. Mag.*, 2002, **82A**(10), 2013–2029.
17. Wolf, B., Inference of mechanical properties from instrumented depth sensing indentation at tiny loads and indentation depths. *Cryst. Res. Technol.*, 2000, **35**(4), 377–399.
18. Oliver, W. and Pharr, G., An improved technique for determining hardness and elastic modulus using load and displacement sensing indentation experiments. *J. Mater. Res.*, 1992, **7**(6), 1564–1583.
19. Oliver, W. and Pharr, G., Measurement of hardness and elastic modulus by instrumented indentation: advances in understanding and refinements to methodology. *J. Mater. Res.*, 2004, **19**(1), 3–20.
20. Pharr, G. M., Strader, J. H. and Oliver, W. C., Critical issues in making small-depth mechanical property measurements by nanoindentation with continuous stiffness measurement. *J. Mater. Res.*, 2009, **24**(3), 653–666.
21. Bhattacharya, A. K. and Nix, W. D., Analysis of elastic and plastic deformation associated with indentation testing of thin films on substrates. *Int. J. Solids Struct.*, 1988, **24**, 1287–1288.
22. Mencik, J., Munz, D., Quandt, E., Weppelmann, E. R. and Swain, M. V., Determination of elastic modulus of thin layers using nanoindentation. *J. Mater. Res.*, 1997, **12**(9), 2475–2484.
23. Ovaert, T., Kim, B. and Wang, J., Multi-parameter models of the viscoelastic/plastic mechanical properties of coatings via combined nanoindentation and non-linear finite element modeling. *Prog. Org. Coat.*, 2003, **47**(3–4), 312–323.
24. Xu, Z. H. and Rowcliffe, D., Finite element analysis of substrate effects on indentation behaviour of thin films. *Thin Solid Films*, 2004, **447**, 399–405.
25. Martin, C. L. and Bordia, R. K., The effect of a substrate on the sintering of constrained films. *Acta Mater.*, 2009, **57**(2), 549–558.
26. Chen, S., Liu, L. and Wang, T., Size dependent nanoindentation of a soft film on a hard substrate. *Acta Mater.*, 2004, **52**, 1089–1095.
27. Pelletier, H., Krier, J. and Mille, P., Characterization of mechanical properties of thin films using nanoindentation test. *Mech. Mater.*, 2006, **38**, 1182–1198.
28. Soh, M., Fischer-Cripps, A., Savvides, N., Musca, C. and Faraone, L., Nanoindentation of plasma-deposited nitrogen-rich silicon nitride thin films. *J. Appl. Phys.*, 2006, **100**(2), 024310.
29. Marshall, D. B., Lawn, B. R. and Evans, A. G., Elastic–plastic indentation damage in ceramics: the lateral crack system. *J. Am. Ceram. Soc.*, 1982, **65**, 561–566.
30. Lawn, B. R. and Evans, A. G., Elastic–plastic indentation damage in ceramics: the median/radial crack system. *J. Am. Ceram. Soc.*, 1980, **63**, 574–581.
31. Zhang, W. and Subhash, G., An elastic–plastic-cracking model for finite element analysis of indentation cracking in brittle materials. *Int. J. Solids Struct.*, 2001, **38**(34–35), 5893–5913.
32. Cook, R. F. and Pharr, G. M., Direct observation and analysis of indentation cracking in glasses and ceramics. *J. Am. Ceram. Soc.*, 1990, **73**, 787–817.
33. Musil, J. and Jirout, M., Toughness of hard nanostructured ceramic thin films. *Surf. Coat. Technol.*, 2007, **201**, 5148–5152.
34. Hu, X. and Lawn, B., A simple indentation stress–strain relation for contacts with spheres on bilayer structures. *Thin Solid Films*, 1998, **322**, 225–232.
35. Jung, Y. G., Lawn, B., Martyniuk, M., Huang, H. and Hu, X., Evaluation of elastic modulus and hardness of thin films by nanoindentation. *J. Mater. Res.*, 2004, **19**(10), 3076–3080.
36. Buckle, H., In *The Science of Hardness Testing and its Research Applications*, ed. J. W. Westbrook and H. Conrad. American Society for Materials, Metals Park, OH, 1973, p. 453.
37. Tsui, T. Y. and Pharr, G. M., Substrate effects on nanoindentation mechanical property measurement of soft films on hard substrates. *J. Mater. Res.*, 1999, **14**, 292–301.
38. Taylor, J. A., The mechanical properties and microstructure of plasma enhanced chemical vapor deposited silicon nitride thin films. *J. Vac. Sci. Technol. A*, 1991, **9**(4), 2464–2468.
39. Petersen, K. E., Dynamic micromechanics on silicon—techniques and devices. *IEEE Trans. Electron Dev.*, 1978, **ED25**(10), 1241–1250.
40. Huang, H., Winchester, K. J., Suvorova, A., Lawn, B. R., Liu, Y., Hu, X. Z. *et al.*, Effect of deposition conditions on mechanical properties of low-temperature PECVD silicon nitride films. *Mater. Sci. Eng. A*, 2006, **435–436**, 453–459.